Bidirectional reflectance measurement of tungsten samples to assess reflection model in WEST tokamak

M. Ben Yaala,[1, 2, a)] M-H. Aumeunier,[3] R. Steiner,[1] M. Schönenberger,[4] C. Martin,[5] M. Le Bohec,[3] C. Talatizi,[3] L. Marot,[1] and E. Meyer[1]

[1)]*Department of Physics, University of Basel, Klingelbergstrasse 82, CH-4056 Basel, Switzerland*

[2)]*Department of Biomedical Engineering, University of Strathclyde, Glasgow G1 1QE, United Kingdom*

[3)]*CEA, IRFM, F-13108 Saint-Paul-Lez-Durance, France*

[4)]*Nano Imaging Lab, Swiss Nanoscience Institute, University of Basel, Klingelbergstrasse 82, 4056 Basel, Switzerland*

[5)]*School of Theoretical and Applied Science, Ramapo College of New Jersey, Mahwah, NJ 07430, USA*

(Dated: 10 August 2021)

This paper presents the measurement of the Bidirectional Reflectance Distribution Function (BRDF) of tungsten (W) samples and the resulting reflection models in the nuclear fusion device WEST (tokamak). For this, an experimental gonio-spectrophotometer was developed to fully characterize the material optical and thermal-radiative properties of metallic samples with different roughness. A ray-tracing photonic simulation was then used to predict the photon behavior in a fully metallic environment as a function of reflectance measurement. Low emissivity (0.1 at 4 μm) and highly specular reflectance (fitting with a Gaussian distribution around the specular direction with small width lower than 10°) are found for W samples. These measurements have been used as input for the photonic simulation and the resulting synthetic image reproduced well the reflection features on the upper divertor detected in WEST infrared experimental images.

I. INTRODUCTION

Infrared thermography is a reliable and robust method widely used in fusion reactors to monitor and protect the plasma-facing components (PFCs) by measuring in real-time their surface temperature. Unlike carbon wall previously used in fusion devices, the future fusion reactor, also called tokamaks, will be fully metallic.

In particular, the ITER fusion tokamak PFCs will be made of beryllium and tungsten which makes the analysis of the infrared (IR) thermography measurement more complicated. Indeed, due to their low and variable emissivity (ranging from 0.1 to 0.5), the contribution of the reflected flux in the total collected photon flux by the IR camera will not be negligible anymore and could be even dominant[1–4]. It was reported that the contribution of the reflected flux from the upper port visible/infra red system of ITER can lead to overestimation of the surface temperature of up to 20 % for the hottest targets and up to 90 % for the coldest surfaces[1]. These false hotspots resulting from the incorrect interpretation of the IR measurements could lead to excessive interruptions of the plasma shots as well as to limitations on scenario development towards high performance.

Photonic simulation capable of predicting accurately the contribution of reflected flux within the collected flux by the camera has been also developed in order to be able to discriminate the parasitic light reflections to other thermal events[5–7]. This has shown that the finest knowledge of optical and thermal-radiative properties of materials is essential to understand well and predict the photon behavior in fully reflective and radiative environment.

This paper presents an experimental setup developed to characterize fully the bidirectional reflectance distribution function of material samples. Directional and total emissivities are also deduced by indirect measurements. The results are presented for tungsten samples at different roughness. Tungsten is the material chosen for the most critical component in the tokamak (divertor) and which is exposed to the highest heat loads and for which the roughness can be changed during the experimental campaign (erosion/deposition phenomena). The relation between reflectance/emittance and roughness is also discussed in this paper. Experimental results are then used as input for the photonic simulation and the resulting IR synthetic image is compared with the experimental image of WEST tokamak.

II. RAY-TRACING PHOTONIC SIMULATION

The photonic simulation code is based on a Monte Carlo ray-tracing (SPEOS CAA V5 Based software from ANSYS-SPEOS[8]) capable of propagating the ray through the complex geometry of tokamak and to take into account the multiple inter-reflections of the ray in the vacuum vessel.

As output, the simulation delivers two images: the "real" image that reproduces the IR camera view and includes the reflected flux from the metallic walls and the "reflection-free" image resulting from materials emission only. The reflection-free image is, therefore, used to quantify the contribution of the reflected light from PFCs and evaluate the real surface temperature. To do so, the simulation is based on three input models, including the thermal scene model, the camera

[a)]Electronic mail: marwa.ben-yaala@strath.ac.uk

FIG. 1. Illustration of the reflectivity model as a combination of Lambertian, specular and Gaussian components. (left) Beam geometry (right) BRDF of each component.

and optics models and photon-materials interaction model. While the thermal model presents the 3D distribution of the heat flux on PFCs and their resulting surface temperature, the optical model includes the camera geometrical parameters (field-of-view (FOV), image size in the focal plane and wavelength range) to reproduce the camera view. The accuracy of simulated results will depend on the accuracy of each model used as input for ray-tracing code. The study in this paper aims to improve the model of photon-materials interaction from experimental measurements of a particular optical material property known as the bidirectional reflectance distribution function.

III. SURFACE REFLECTANCE MODEL

The reflected light behavior is described with a combination of three main components shown in Figure 1: a Lambertian, a specular and Gaussian reflectance so-called also glossy reflection. Lambertian reflection, occurs with an equal spread of reflecting light in all directions from a surface. Specular reflection occurs with a directional reflection of light from the surface, with an incident angle equal to reflection angle defined by Snell - Descartes laws. In practice, most of the specular material's reflection is a combination of a pure major directional specular component with a diffuse component following a Gaussian model, for which the reflected light has a Gaussian probability of being reflected with a particular angle around the main direction.

Reflection models are described through a BRDF that relates the energy arriving at a surface from the direction of illumination to the reflected intensity in the direction of the detector:

$$BRDF(\lambda,\theta_i,\phi_i,\theta_r,\phi_r) = \frac{dL_r(\lambda,\theta_r,\phi_r)}{dE_i(\lambda,\theta_i,\phi_i)} \quad (1)$$

Where λ is the wavelength of the incident light, E_i is the incident spectral irradiance, L_r is the reflection spectral radiance, (θ_i,ϕ_i) is the direction of the incident light and (θ_r,ϕ_r) is the direction of the reflected light presented in Figure 2a).

In order to collect BRDF experimental data, a specialized measurement device called gonioreflectometer is used. The full description of this device and the measuring procedure is described in the following section.

IV. EXPERIMENTAL SECTION

A. BULGO spectrophotometer

1. *Setup description*

Basel University Laboratory GOniospectrophotometer (BULGO) is a device with a four degree of rotational freedom designed to measure the optical properties of materials by measuring the directional reflectance of the sample as a function of angles of illumination and observation. The incident light on a material surface comes from the light source aperture. The light viewed by the detector is delimited by its aperture. Both the direction of illumination (θ_i,ϕ_i) and viewing direction (θ_r,ϕ_r), in spherical coordinates, can vary independently within the hemisphere above the material sample. An overview of this gonioreflectometer is shown in Figure 2b) and 2c)). The instrument consists of:
i) a rotatable and height adjustable sample holder
ii) a vertical half circular arc supporting the zenith motion of the light source
iii) a horizontal circular rail for the azimuthal motion of the light source
iv) a vertical stationary half-circular arc to support the zenith motion of the light collimator.
The light source mounted on the apparatus is a tungsten halogen 50 W Ushio lamp, inside a Lowel assembly of 12.7 cm diameter. The assembly allows two possible settings of the lamp which are 'spot' and 'flood'. Spot position is used for yielding a more parallel light beam, increasing the homogeneity of the illuminated area over oblique illumination angles. In both configurations, the light coming from the lamp is not collimated which implies that it reaches the surface of the sample with different angles. In order to correct the reflected flux from non-parallel rays, a pure specular aluminium reference sample was measured. Its BRDF represents the angular distribution of the light source and it is, therefore, deconvoluted from the BRDF of measured samples to get corrected results describing the pure reflectance of the sample surface. The lamp, which produces 1250 lumen, covers the electromagnetic spectrum in the region of 0.35 to 2.5 μm and provides a sufficiently strong signal for the detector. The detector is composed of a light collimator connected to a spectrophotometer through an optical fiber. The spectrophotometer is an Avantes spectrophotometer (AvaSpec-2048) that measures in the wavelength range from 0.2 to 1.1 μm. The motion and positioning of the BULGO components, as well as the operation of the spectrometer, are remotely controlled by a LabVIEW program. The system is, therefore, able to operate in a fully automatized mode.

FIG. 2. a) BRDF parameters b) and c) Overview of BULGO gonioreflectometer. 1) Sample holder 2) Collimator 3) Optical fiber 4) Light source 5) Spectrophotometer 6) Labview computer software

FIG. 3. BRDF of JET Inconel tile measured by BULGO and FIGOS goniophotometers

2. Alignment process and assembly precision

For BRDF measurement, the sample reflected flux collected by the spectrophotometer is compared to the reference reflectivity (Spectralon, polytetrafluoroethylene). The Spectralon exhibits the highest diffuse reflectance of any known material or coating over the UV-VIS-NIR region of the spectrum. Its deviation from the pure Lambertian reflectance was measured by its manufacturer/supplier and this deviation was translated into a correction factor that is considered in the calculation of the BRDF.

The following section describes the alignment process and its accuracy. The sample holder was adjusted in the horizontal plane in order to align the sample surface with the detector and the light horizontal planes. The sample was then placed in the center of the sample holder and its height was adjusted to the same height of the Spectralon reference in order to measure under the same geometrical configurations.

The focusing of the setup was performed by focusing the detected signal in the optical fiber. This was done by using a laser connected to the end of the optical fiber (instead of the spectrophotometer). The collimator lens position was then varied until reaching the position where the beam footprint does not dependent on the object distance. Due to the reversibility of the optical path, this step permits finding the collimator focal length to get a focused beam inside the optical fiber.

The geometric accuracy of the sensor FOV was tested by placing a sharp thin stick in the collimator position. This was accomplished by moving the stick over the zenith arc that supports the detection system while tracing on graphic millimeter paper the maximal deviations of the stick from the center of the sample holder. The observed deviations among the 6 zenith positions (0° to 75°) were smaller than 1.2 cm in both x and y directions. The same procedure was followed for the zenithal and azimuthal rotation of the light source and a maximum deviation of 0.8 cm was found in both cases.

In order to determine the position of the measurement spot on the sample while the detector is rotating on the zenith arc, the deviation of the collimator FOV across the target was examined by connecting a laser to the end of the optical fiber. The footprint was recorded on millimeter paper for each zenith position of the detector. At zero incidence, the laser footprint on the sample was circular with a 1 cm diameter (corresponding to the collimator diameter) that became distinctively elliptical towards higher zenith angles reaching around 3.9 cm at 75°. This limits the smallest size of samples that can be measured with BULGO to 4 cm with the condition of surface homogeneity over the detection area. The impact of detector footprint variation on the BRDF measurement is cancelled by measuring the reference Spectralon and the sample with the same geometrical configurations.

3. Measurements

A two-hour warm-up period was maintained for both the spectrophotometer and the light source before starting any measurement. The warming-up of the spectrophotometer is essential to stabilize dark current while the warming-up of the light source is used to provide a stable and homogeneous intensity distribution over time.

Any sequence of positions can be programmed and executed from a LabVIEW program and the spectrophotometer detects the reflected intensity from the target surface. The full measurement cycle starts with the measurement of a Spectralon reference followed by a dark current measurement of the spectrophotometer (by closing the collimator aperture) and finally a measurement of the sample under the same geometrical configurations as those used for the Spectralon is done. As also described by Murray-Colman and Smith[9], the sample BRDF is then calculated as follows:

$$BRDF = C_f \times \frac{\frac{I_{sample}}{T_{sample}} - \frac{I_{dark}}{T_{dark}}}{\frac{I_{Spectralon}}{T_{Spectralon}} - \frac{I_{dark}}{T_{dark}}} \quad (2)$$

where I is the intensity of reflected light detected by the spectrophotometer, T is the integration time automatically adjusted by the program to have enough measured intensity and C_f is the reflectance of the spectralon.

4. Validation

Due to the complexity of the BRDF measurement process and the multiplicity of parameters that can influence the precision of the measurement (stability of the light source, stability of the spectrophotometer and its dark measurement, angular positioning on 4 axes, etc.), the measurement error cannot be calculated precisely. However, another way to estimate this error is by measuring a specific sample with another goniospectrophotometer and compare the results to BULGO measurements. For that, an Inconel tile sample from JET tokamak[10] was measured and compared to the results obtained with the Field Goniometer System FIGOS at the University of Zürich, Switzerland[11].

The measurement position sequence was the following: the sample holder was fixed at 0°, the light position at 10° and 0° in the zenith and azimuth directions respectively and the

FIG. 4. a) W samples mechanically polished to different roughness b) a picture to show their mirror reflections and c) d) their corresponding surface topography measured by Laser Scanning Confocal Microscopy (LSCM)

spectrometer was moved on its zenith supporting arc by a step of 15°. BRDF results obtained for both systems are shown in Figure 3. Both devices deliver very similar BRDF values for the same sample with a 2.1% maximum difference between both measurements confirming the accuracy of the BULGO system.

B. Further characterization techniques

Using BULGO, the bidirectional reflectance of a surface cannot be measured for some angular combinations of the light source and detector. In particular, the 0° light source zenith position over the 0° sensor position is a "blocked" angular combination due to the shadow casting effect on the sample. This artifact is attributed to the sensor being directly underneath the light source. Furthermore, the high grazing angle (in the range of 80 to 90°) cannot be measured due to mechanical restrictions. Different methods are thus required to extrapolate the full BRDF at these extreme geometrical configurations.

The 0 degree incidence normal reflectance was measured using a UV-vis-near infrared (NIR) spectrophotometer Varian Cary 5 equipped with a 110 mm diameter integrating sphere under nearly normal incidence (3°20') in the wavelength range of 0.25–2.5 μm[12]. An integrating sphere is designed to collect reflected radiation (diffuse or total) from a sample. It consists of a spherical cavity with a polytetrafluoroethylene coating of high diffuse reflectance on its inner wall. The sample reflects the incident light, which is repeatedly reflected by the spherical cavity's inner wall. This produces diffuse light which enters the detector. The measurement with this spectrophotometer does not allow to measure the pure specular reflectivity part due to the sphere aperture which includes the reflected flux around the specular direction (+/-1°6).

To measure the pure specular reflectivity, a third setup is used consisting of a spectral ellipsometer (Sentech SE 850). This measures the ellipsometric parameters (Ψ, Δ) in the range of 0.3-2.3 μm for angles of incidence of 45, 55 and 65°. Δ is the phase difference induced by the reflection and Ψ is the amplitude component (tanΨ is the amplitude ratio upon reflection). The fit of these six data sets (fitting routine SpectraRay) using a fixed refractive index and absorption model were performed to obtain the optical constants (refractive index n and extinction coefficient k) of the surface as a function of the wavelength. The pure specular reflectivity of the surface at normal incidence was then recalculated using these optical constants[12].

The specular reflectance of samples was also measured using a commercial Bruker Vertex 70 Fourier Transform IR (FTIR), with extended spectral ranges, from 100 cm^{-1} (100 μm) to 20,000 cm^{-1} (0.5 μm). The far and mid-infrared measurements were performed using a combination of broadband beam splitter, high power IR source (globar lamp) and deuterated-triglycine sulfate detector, while for near-IR and visible a combination of a quartz beam splitter, a high power tungsten lamp and a silicon diode detector. A specular reflection/transmission stage (A510/Q-T) with a fixed angle of incidence of 11° was used in conjunction with FTIR spectrometer. The beam size was between 1 and 1.5 mm, focused close to the center of the sample.

To explore how the roughness of the sample affects the measured BRDF, the surface roughness of the samples was also measured using a three-dimensional laser scanning confocal microscope (3D LSCM, VK-X1100, Keyence). An objective lens of 20 times magnification was used to reconstruct the surface topography. The arithmetical mean height of the surface is calculated over an area of 531 $\times$ 708 μm.

V. RESULTS AND DISCUSSION

A. BRDF results for W samples with different surface topography

The plasma-facing components are submitted to high heat flux and others erosion-deposition phenomena causing a change of the materials surface state (oxidation) and roughness. This paper focuses on the impact of roughness on BRDF. To investigate the effect of surface roughness on the BRDF, four W samples M100-M103 (shown in Figure 4) were prepared by mechanical polishing to achieve several roughnesses. The results of their measured average roughness Ra are displayed in figure 4.

The total and diffuse reflectivity were measured in the range 0.25-2.5 μm. This allows us to plot the specular reflectivity in the inset of Figure 5 (dotted line) on the right side. On that same figure is displayed the specular reflectivity measured by an FTIR in the range 0.5-100 μm. A good agreement between both spectrophotometers is demonstrated. Interestingly, for samples M102 and M103, in the range 0.25-4.6 μm the specular reflectivity is not following the corresponding roughness measurements i.e. decrease of specular reflectivity for increasing roughness. In fact, it is possible to calculate the specular reflectivity with the well-known Bennett's formula[13], which correlates the specular reflectivity at normal incidence with the surface roughness:

$$R_s = R_0 \times \exp\left(\frac{-(4 \times \pi \times RMS)}{\lambda^2}\right)^2 \quad (3)$$

where R_s is the resulting specular reflectivity, R_0 is the reflectivity of an ideally smooth surface of the same material, RMS is the root mean square roughness, and λ is the wavelength of light. The formula describes a decline of the reflection as a function of the RMS roughness of the surface.

FIG. 5. Total, diffuse and specular reflectivities measured for the W samples M100-M103. Reflectivity of W samples measured by the integrating sphere (dashed lines) and FTIR (solid lines). In the inset are plotted both measurements in the range 0.25 to 5 μm. Reflectivity values at 4 μm are displayed in the inset.

FIG. 6. M100 reflectivities at 40°, 60°, 70°, and 80° for s and p polarizations at 0.65 μm (triangle symbol). The solid lines represent the s and p components fitted from n and k.

FIG. 7. W samples normalised BRDF results for λ=0.9 μm and variable incident angle

FIG. 8. W samples FWHM variation as a function of the wavelength (data extracted from figure 7).

At a perfectly smooth surface (RMS=0) the reflectivity equals the square of the Fresnel reflection. Goossens, et.al.[14], described a nearly perfect agreement for smooth samples, for the rougher samples the deviation between experiment and model is larger. Even though the same trend is still visible, the Benett's formula becomes inadequate to predict the specular reflectivity as the surfaces become rougher.

The reflectivity of M102 and M103 follow the Bennett's formula only for wavelength values higher than 4.6μm. As seen in Figure 4 the scratches on the surface of sample M102 have a width less than 4.6 μm and always contribute to scatter the light below this wavelength. For M103 the surface at high wavelength is affected by large holes (>50 μm) but for wavelength below 4.6 μm the surface is less scratched in comparison to M102.

Reflectivity measurements were performed using an ellipsometer at incidence angles of 40°, 60°, 70°, and 75°, for s and p polarized lights on the sample M100. S and p reflectivities are plotted for a wavelength of 0.65 μm in Figure 6. The full line in Figure 6 represents the s and p components calculated with the theoretical optical constants[15] using the Fresnel equation. The refractive index (n) and extinction coefficient (k) for this film are 2.4 and 2.9, respectively, at 0.65 μm. In Figure 6 the value at 0° is the one measured with the spectrophotometer (Cary setup). The measured value with Cary is quite in agreement with ellipsometer measurement. At 90° the value is extracted from the calculated curve. This value is equal to 100% indicating that the material surface is fully specular at grazing angle.

For all tested surfaces, the BRDFs were measured in the plane of incidence (ϕ_i=ϕ_r=0) and in the orthogonal plane (ϕ_i=0; ϕ_r=90) and over the reflection hemisphere (variable θ_i and θ_r). In this way, it is shown that the W samples BRDF is independent of the sample rotation.

BRDF results for the four W surfaces are presented in figure 7. The BRDF is plotted versus the detection angle for different incident angles at a fixed wavelength of 0.9 μm. The black line curves represent the measurement results while the red line is for the corrected measurement by subtracting the effect of a non-collimated light source. All results were fitted with a Gauss function centred at the specular direction (θ_i=θ_r) represented in the figure by a dashed line. No constant reflectance component was measured. This indicates that both samples have only a pure Gaussian reflectance around the specular and do not present any Lambertian (or diffuse) component (presented by the offset in Figure 1). Besides, for all samples, the BRDF increases towards grazing angles.

The Gaussian Full Width at Half Maximum (FWHM) at 15° incidence angle is plotted in Figure 8 for wavelength values ranging from 0.25 to 1.1 μm. The FWHM stayed almost constant in the entire range and all values are below 10 degrees. As explained previously for the diffuse and roughness correlation of the M102 and M103, the FWHM of the latest is lower than M102. For samples M100 and M101, representing the smallest Ra values (0.015 and 0.045 μm respectively) the FWHM is around 2°. This value is around 4-5 times higher for the rough samples M102 and M103.

Su et. al.[16], adopted in their BRDF model the optical roughness instead of surface roughness. The optical roughness (σ_{opt}) can be expressed as the ratio between surface roughness (σ_0) and wavelength (λ):

$$\sigma_{opt} = \frac{\sigma_0}{\lambda} \tag{4}$$

According to both studies Su et. al.[16] and Wen et. al.[17], the surface can be classified in 3 regions following to the surface roughness: (i) Specular region when $0 < \sigma_{opt} < 0.2$ for which Bennett Law can be applied to get directional reflectivity (ii) Intermediate region when $0.2 < \sigma_{opt} < 1$ or which approximate models are needed to describe BRDF (iii) Geometric region when $\sigma_{opt} > 1$ for which geometric optics law can be used. Su et al.[16] presented a plot of the BRDF for five incidence angles and three optical roughness values: 0.1, 0.2 and 0.3 for a pure specular surface. As seen in figure 7 reported by Su et al.[16], the maximum of the BRDF value is increasing for increasing angle and the FHWM is increasing for higher σ_{opt}. For = 0.9 μm (wavelength at which the BRDF is presented in Figure 7), the σ_{opt} values are 0.063, 0.2, 0.59 and 1.24 for M100, M101, M102 and M103, respectively.

Theoretical models like Torrance and Sparrow[18] assume the reflection of incident radiation to be specular for σ_{opt} below 1 or even below 0.2 like for Wen and Mudawar[17]. For our samples M100, M101 and M102, the σ_{opt} is below 1 and only M100 and M101 have a σ_{opt}<0.2.

FIG. 9. Spectral normal emissivity as a function of wavelength for M100 to M103 samples

FIG. 10. W reference samples n factor fitted from the n cosine power model of the directional emissivity.

B. Emissivity model

Using Kirchhoff's Law, the spectral normal emissivity of W reference samples is directly calculated from spectral directional hemispherical total reflectance measured by the integrating sphere and FTIR (presented in Figure 5). Results are shown is Figure 9. As can be seen, the emissivity increases with roughness for the entire wavelength range. The only exception is for the samples M101. That would suggest that the average roughness parameter is not able to describe all the complex features on the surface. Others measures of the roughness seems to include others complex features on the surface: high amplitude, low frequency (scratches) , correlation length (machining)[19,20]. For all samples, the emissivity decreases with increasing wavelength, in particular, a drop by a factor 5 from the visible ($\lambda < 0.8\ \mu$m) to IR range ($\lambda > 2.5\ \mu$m) is measured for the samples M100.

The integration of the BRDF over a hemispherical solid angle gives the spectral hemispherical reflectance at a given incidence angle (ρ(i)). The spectral directional emissivity at a given emission angle (ε(e)) can be then deduced using Kirchhoff's law: ε(e)=1-ρ(i). The emission angular dependence is described with a cosine n power model: n=1 is for Lambertian distribution; for n>1, emission will be concentrated around the normal of surface, and for n<1, the emission is more evenly distributed across all emission angles with non-negligeable contribution of high emission angles (so-called "grazing angles"). The n coefficient results are presented in Figure 10. For samples M101, M102 and M103, the n coefficient is found lower than 1 in the visible range favouring grazing angle.

C. Simulation results

The main infrared source in tokamak comes from the heat flux deposited on the plasma-facing components and in particular on the lower divertor which is situated at the bottom of the vacuum vessel and receives the maximum heat flux up to 10 MWm^2 (steady-state) and 20 MW/m^2 (slow transients). The plasma is transparent in IR range. The WEST thermography system has been designed to operate at 3.9 μm ($\pm$100 nm) to monitor a wide temperature range from 90°C to 3400°C (melting temperature of tungsten). In the simulation, only the IR source coming from the divertor is considered (turned on) to assess the reflections coming from these components. Figure 11 compares the experimental image of WEST Wide Angle Tangential view with the simulated ones by considering two scenarios of a full diffuse surface for in-vessel components (in emission and reflectance) and high specular surface roughly adjusted to W sample measurements (M103). Table I summarizes the parameters roughly adjusted to laboratory measurement used as input for the photonic simulation. Similar reflections features are observed on experimental and simulated images, especially on upper divertor, when considering specular reflectance roughly adjusted to experimental data. It is worth noting that others physical phenomenon are involved and not completely modeled (as the bubble on the floor), which explains the quantitative difference between the simulated and experimental images. Further analysis of the experimental data shows that the emission model is not (spatially) uniform on the same components during the WEST experimental campaign (depending to erosion/deposition phenomena by plasma). Further simulation should take into account the emissivity variation and check if the associated reflectance model (BRDF) is also affected.

VI. CONCLUSION

This paper presented an accurate experimental tool available for the optical properties measurements of PFC materials mainly the bidirectional reflectance distribution function. BULGO was developed for this purpose and showed, after calibration, good accuracy in comparison to another setup (FIGOS). BRDF first results of the W samples with different surface topography show that their reflectance is represented by a pure Gaussian component around the specular direction with an angular width of less than 10°. The angular dependence of emissivity can be fitted with a cosine n power model. On the other hand, the Gaussian FWHM was found almost constant with the wavelength. It is found that roughness has an impact on BDRF of samples but it does not represent the only factor to describe it.

Experimental data were implemented in the ray-tracing software SPEOS in order to have a better interpretation of the images of WEST camera and distinguish the patterns caused by the reflection of W divertor. By comparing simulated and experimental images in WEST, the experimental results were confirmed including the Gaussian response and the angular dependence of reflectance of the W divertor material.

ACKNOWLEDGMENTS

This work has been carried out within the framework of the EUROfusion Consortium and has received funding from the Euratom research and training program 2014–2018 and 2019–2020 under Grant Agreement No. 633053. The views and opinions expressed herein do not necessarily reflect those of the European Commission. The authors would like to thank the Swiss Federal Office of Energy, the Swiss Nanoscience Institute, the Swiss National Science Foundation and the Federal Office for Education and Science for their financial support. We thank Juerg Schopfer, from the Remore Sensing Laboratories, Department of Geography, University of Zurich, for the measurements using FIGOS.

FIG. 11. (Left) Infrared experimental image of WEST Wide Angle Tangential View [3300-3400 nm filter band] (Middle) Simulated image assuming high specular surface further to W sample measurement in laboratory and (Right) Simulated image assuming all diffuse surface.

WEST components	**Materials**	**MEASUREMENT**				**Parameters used for simulation**		
		***Ra* (μm)**	***Emissivity* @ 4 μm**	***N power Emissivity***	***Reflectance model @ 2 μm***	***Emissivity***	***N power emissivity***	***Reflectance***
Lower Divertor	W-coated graphite	1.8 1.1 (M103)	0.03 0.09 (M103)	– N=1.5	Specular but with max R shifted Highly Specular (8°)	0.1	1	Specular (7°) Specular (7°)
Baffle	W-coated graphite	-	-		-	0.1	1	Specular (7°)
Inner bumper	W-coated CFC (PVD)	3.2 6.2	0.16 0.09	–	Specular but with max R shifted	0.15	1	Specular (7°)
Outer bumper (LPA)	W-coated CFC (PVD)	3200 nm	0.16	–		0.15	1	Specular (7°)
Upper divertor	W-coated CuCrZr	-	-	–	-	0.1	1	Specular (7°)
Heating antenna bumper	W-coated CFC (VPS)	-	-	-	-	0.15	1	Specular (7°)

TABLE I. Input parameters for the SPEOS simulation.

VII. AVAILABILITY OF DATA

The data that support the findings of this study are available from the corresponding author upon reasonable request.

VIII. REFERENCES

[1]M.-H. Aumeunier, M. Firdaouss, J.-M. Travère, T. Loarer, E. Gauthier, V. Martin, D. Chabaud, E. Humbert, and J. E. T.-E. F. D. A. Contributors, "modeling of the iter-like wide-angle infrared thermography view of jet," Review of Scientific Instruments **83**, 10D522 (2012).

[2]M. H. Aumeunier, Y. Corre, M. Firdaouss, E. Gauthier, T. Loarer, J. M. Travère, and J. L. Gardarein, "multi parametric sensitivity study applied to temperature measurement of metallic plasma facing components in fusion devices," in *2013 3rd International Conference on Advancements in Nuclear Instrumentation, Measurement Methods and their Applications (ANIMMA)* (IEEE, 2013) pp. 1–6.

[3]T. Loarer, "Surface temperature measurement of plasma facing components in metallic environment," Contributions to Plasma Physics **51**, 201–206 (2011).

[4]S. Amiel, T. Loarer, C. Pocheau, H. Roche, M. H. Aumeunier, E. Gauthier, C. Le Niliot, and F. Rigollet, "Surface temperature measurement of plasma facing components with active pyrometry," in *Journal of Physics: Conference Series*, Vol. 395 (IOP Publishing, 2012) p. 012074.

[5]M. Kočan, R. Reichle, M. H. Aumeunier, J. P. Gunn, S. Kajita, F. Le Guern, S. W. Lisgo, T. Loarer, A. S. Kukushkin, A. S. Naik, *et al.*, "first results on modeling of iter infrared images," Physica Scripta **2016**, 014047 (2016).

[6]M.-H. Aumeunier, M. Kočan, R. Reichle, and E. Gauthier, "impact of reflections on the divertor and first wall temperature measurements from the iter infrared imaging system," Nuclear Materials and Energy **12**, 1265–1269 (2017).

[7]S. Kajita, M.-H. Aumeunier, E. Yatsuka, A. Alekseev, E. Andreenko, A. Kukushkin, V. Neverov, M. Kocan, M. Bassan, E. Veshchev, *et al.*, "effect of wall light reflection in iter diagnostics," Nuclear Fusion **57**, 116061 (2017).

[8]`https://www.ansys.com/products/optical/ansys-speos`.

[9]J. Murray-Coleman and A. Smith, "The automated measurement of brdfs and their application to luminaire modeling," Journal of the Illuminating Engineering Society **19**, 87–99 (1990).

[10]K. D. Zastrow, S. R. Keatings, L. Marot, M. G. O Mullane, G. De Temmerman, and J. E. Contributors, "Modeling the effect of reflection from metallic walls on spectroscopic measurements," Review of Scientific Instruments **79**, 10F701 (2008).

[11]J. Schopfer, S. Dangel, M. Kneubühler, and K. Itten, "The improved dual view field goniometer system figos," Sensors **8**, 5120–5140 (2008).

[12]B. Eren, L. Marot, M. Wisse, D. Mathys, M. Joanny, J.-M. Travère, R. Steiner, and E. Meyer, "In situ evaluation of the reflectivity of molybdenum and rhodium coatings in an ITER-like mixed environment," Journal of Nuclear Materials **438**, S852–S855 (2013).

[13]H. E. Bennett, M. Silver, and E. J. Ashley, "Infrared reflectance of aluminum evaporated in ultra-high vacuum," JOSA **53**, 1089–1095 (1963).

[14]V. Goossens, N. Gotzen, S. Van Gils, E. Stijns, G. Van Assche, R. Finsy, and H. Terryn, "Predicting reflections of thin coatings," Surface and Coatings technology **204**, 551–557 (2009).

[15]E. D. Palik, *Handbook of optical constants of solids*, Vol. 3 (Academic press, 1998).

[16]P. Su, Q. Eri, and Q. Wang, "optical roughness brdf model for reverse monte carlo simulation of real material thermal radiation transfer," Applied optics **53**, 2324–2330 (2014).

[17]C.-D. Wen and I. Mudawar, "Modeling the effects of surface roughness on the emissivity of aluminum alloys," International journal of heat and mass transfer **49**, 4279–4289 (2006).

[18]K. E. Torrance and E. M. Sparrow, "Theory for off-specular reflection from roughened surfaces," Josa **57**, 1105–1114 (1967).

[19]E. S. Gadelmawla, M. M. Koura, T. M. A. Maksoud, I. M. Elewa, and H. H. Soliman, "Roughness parameters," Journal of materials processing Technology **123**, 133–145 (2002).

[20]M. Aumeunier, J. Gerardin, C. Talatizi, M. Le Bohec, M. B. Yaala, L. Marot, T. Loarer, R. Mitteau, J. Gaspar, F. Rigollet, *et al.*, "Infrared thermography in metallic environments of west and asdex upgrade," Nuclear Materials and Energy **26**, 100879 (2021).

Bidirectional reflectance measurement of tungsten samples to assess reflection model in WEST tokamak

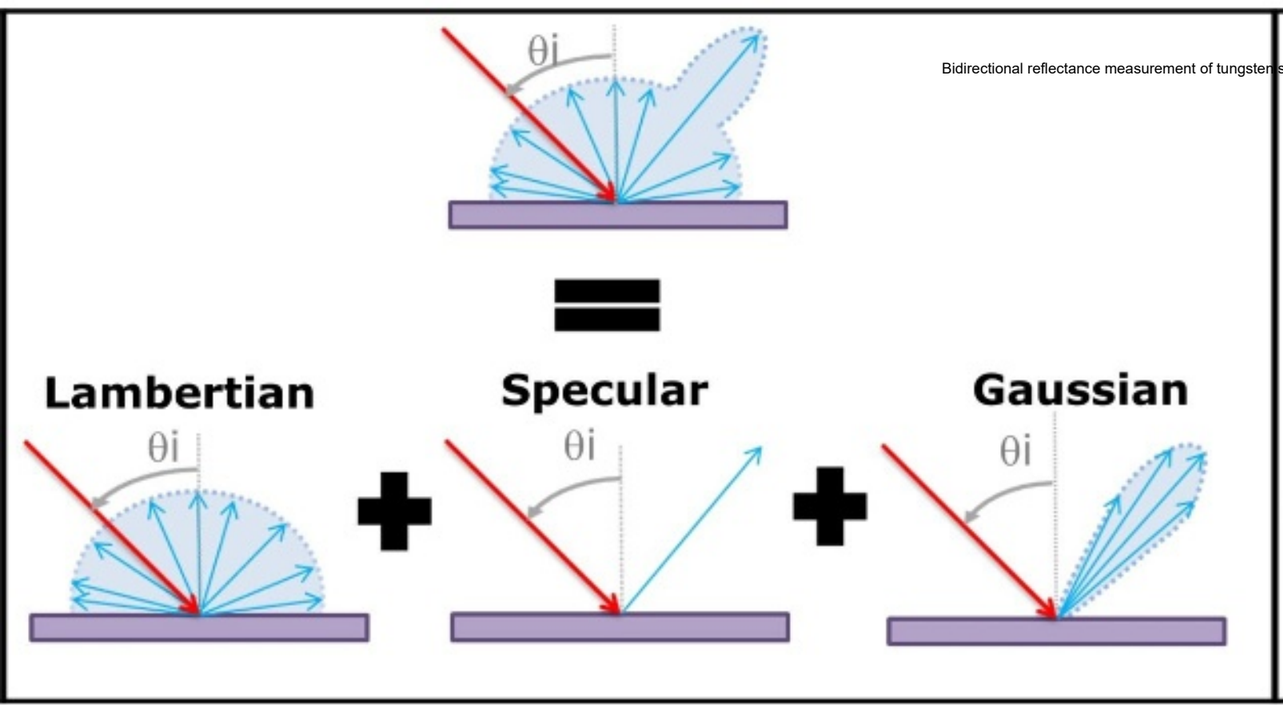

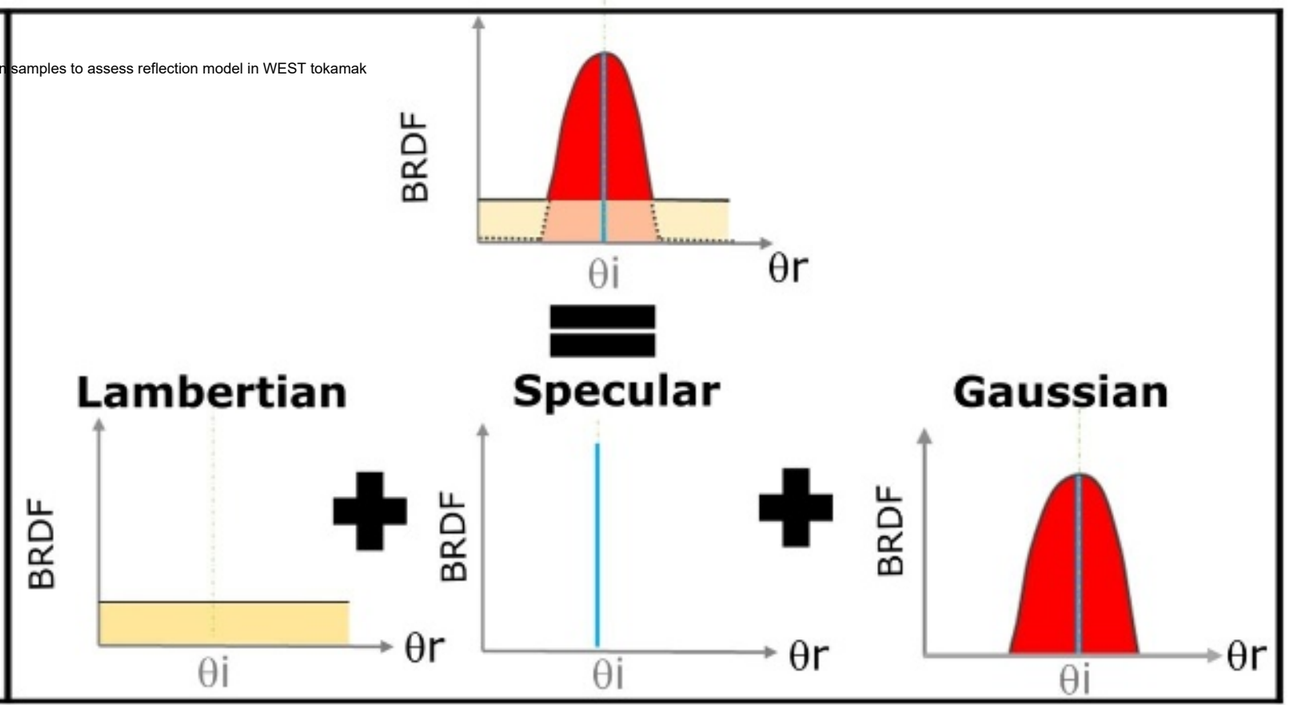

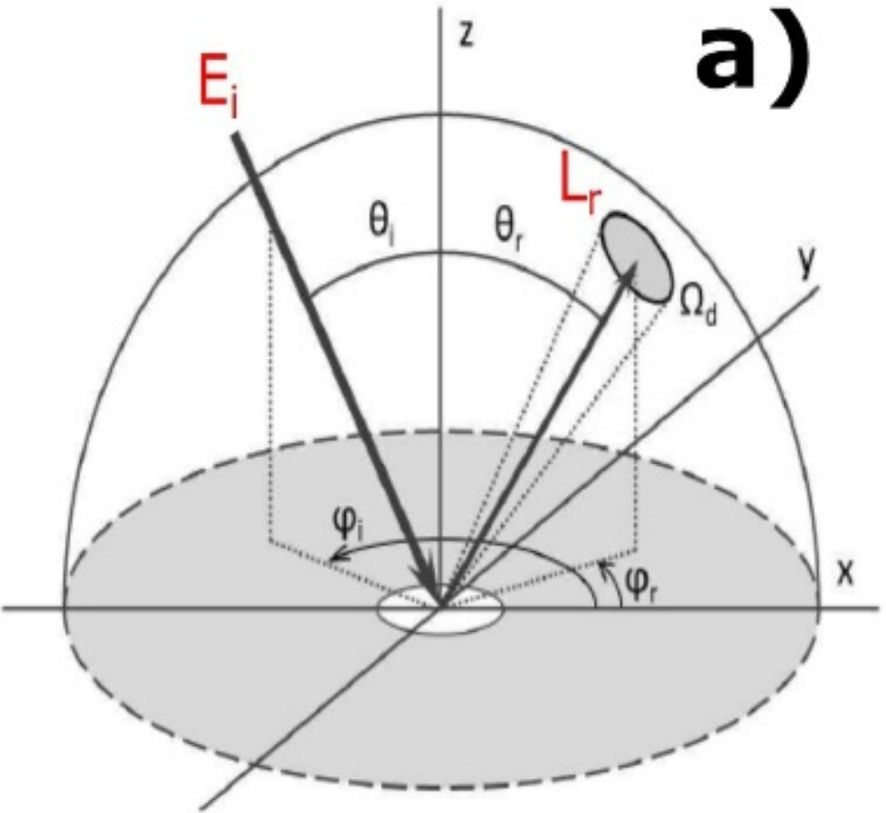
a)
z
E_i
L_r
θ_i
θ_r
Ω_d
y
φ_i
φ_r
x

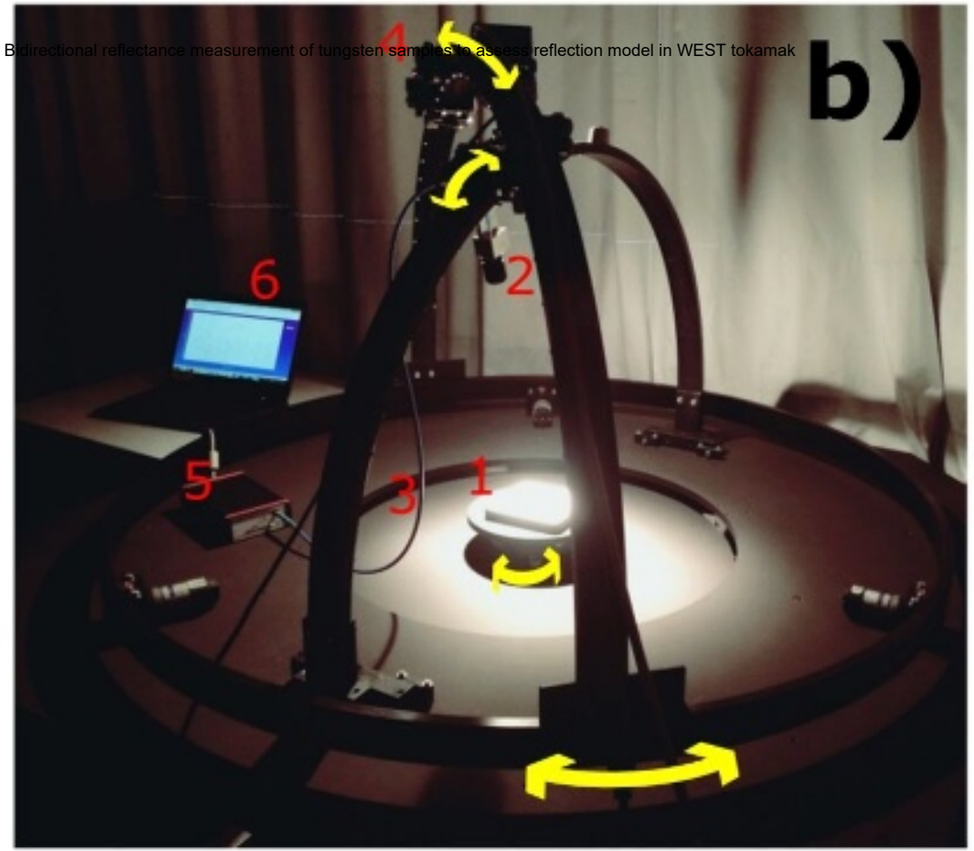
b)
4
2
6
5
3
1

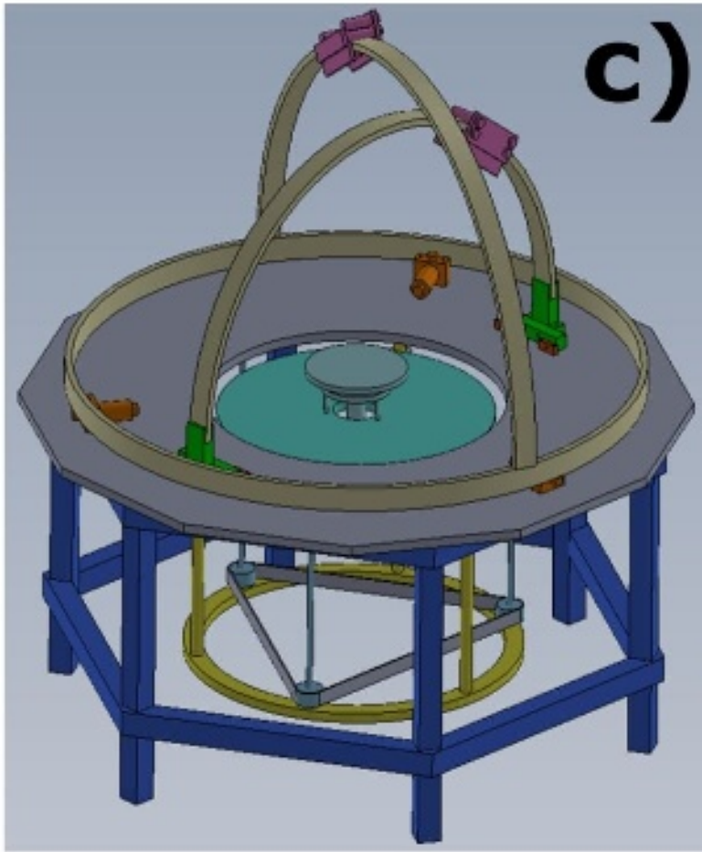
c)

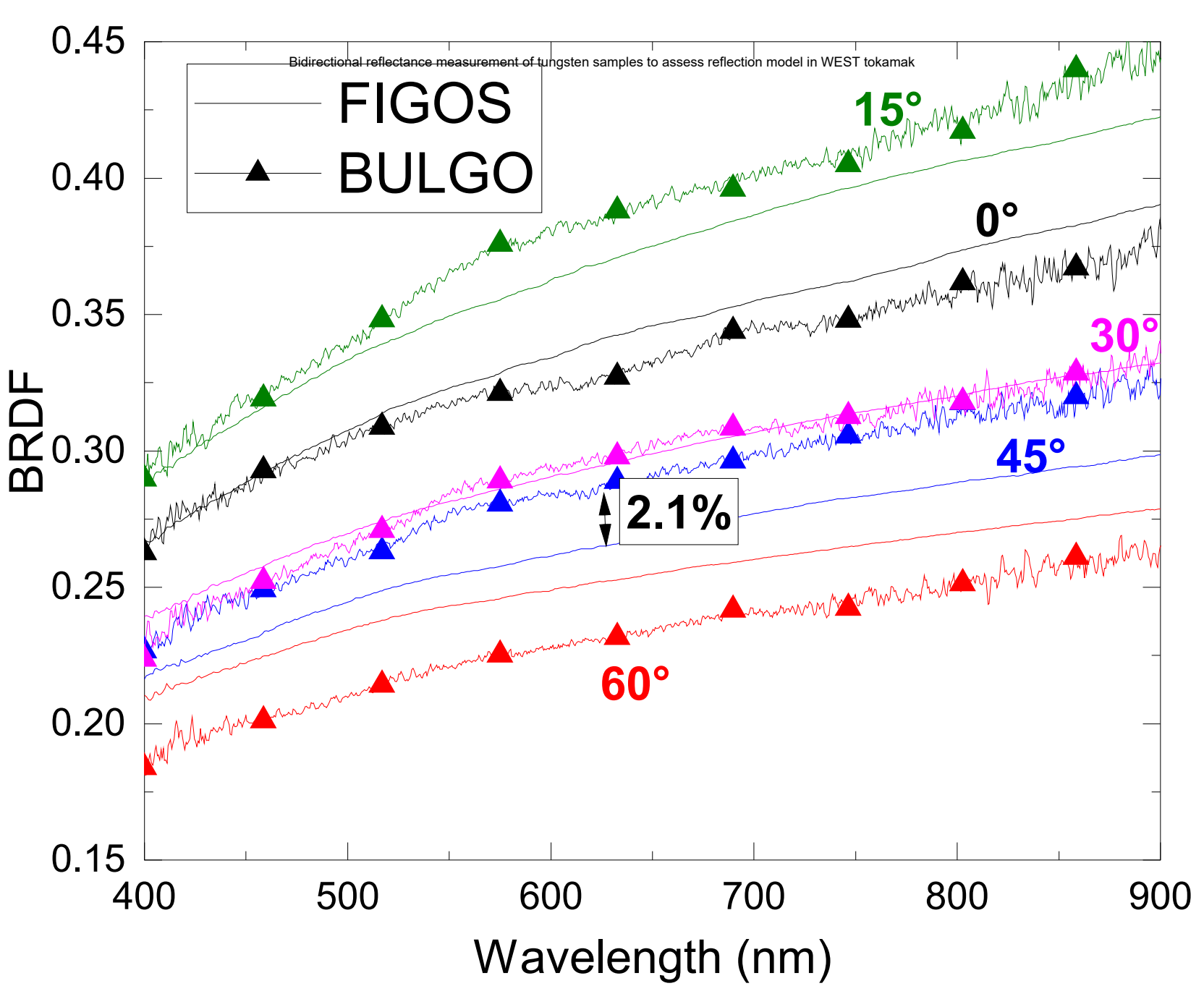
Bidirectional reflectance measurement of tungsten samples to assess reflection model in WEST tokamak
FIGOS
BULGO
15°
0°
30°
45°
60°
2.1%
BRDF
Wavelength (nm)
0.45
0.40
0.35
0.30
0.25
0.20
0.15
400
500
600
700
800
900

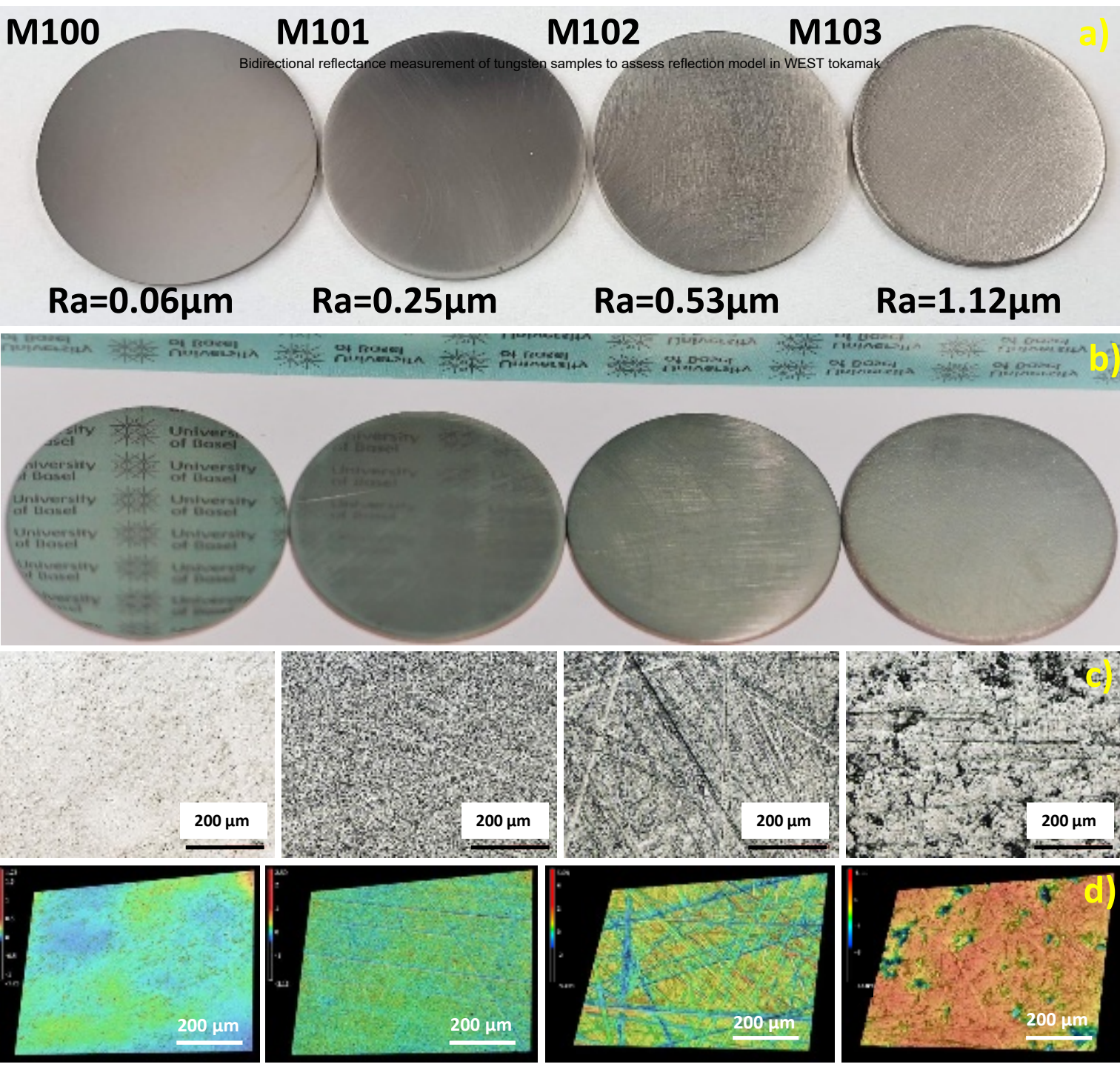
M100
M101
M102
M103
a)
Bidirectional reflectance measurement of tungsten samples to assess reflection model in WEST tokamak
Ra=0.06µm
Ra=0.25µm
Ra=0.53µm
Ra=1.12µm
b)
c)
200 µm
200 µm
200 µm
200 µm
d)
200 µm
200 µm
200 µm
200 µm

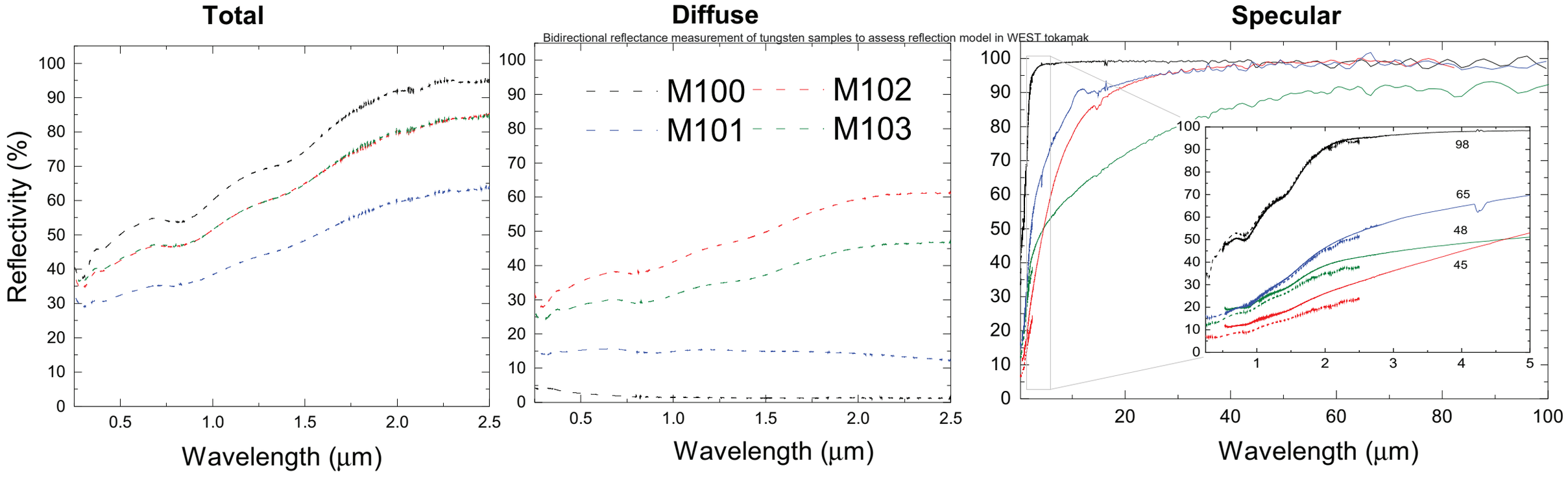
Total
Diffuse
Specular
Bidirectional reflectance measurement of tungsten samples to assess reflection model in WEST tokamak
Reflectivity (%)
Wavelength (μm)
M100
M101
M102
M103
98
65
48
45

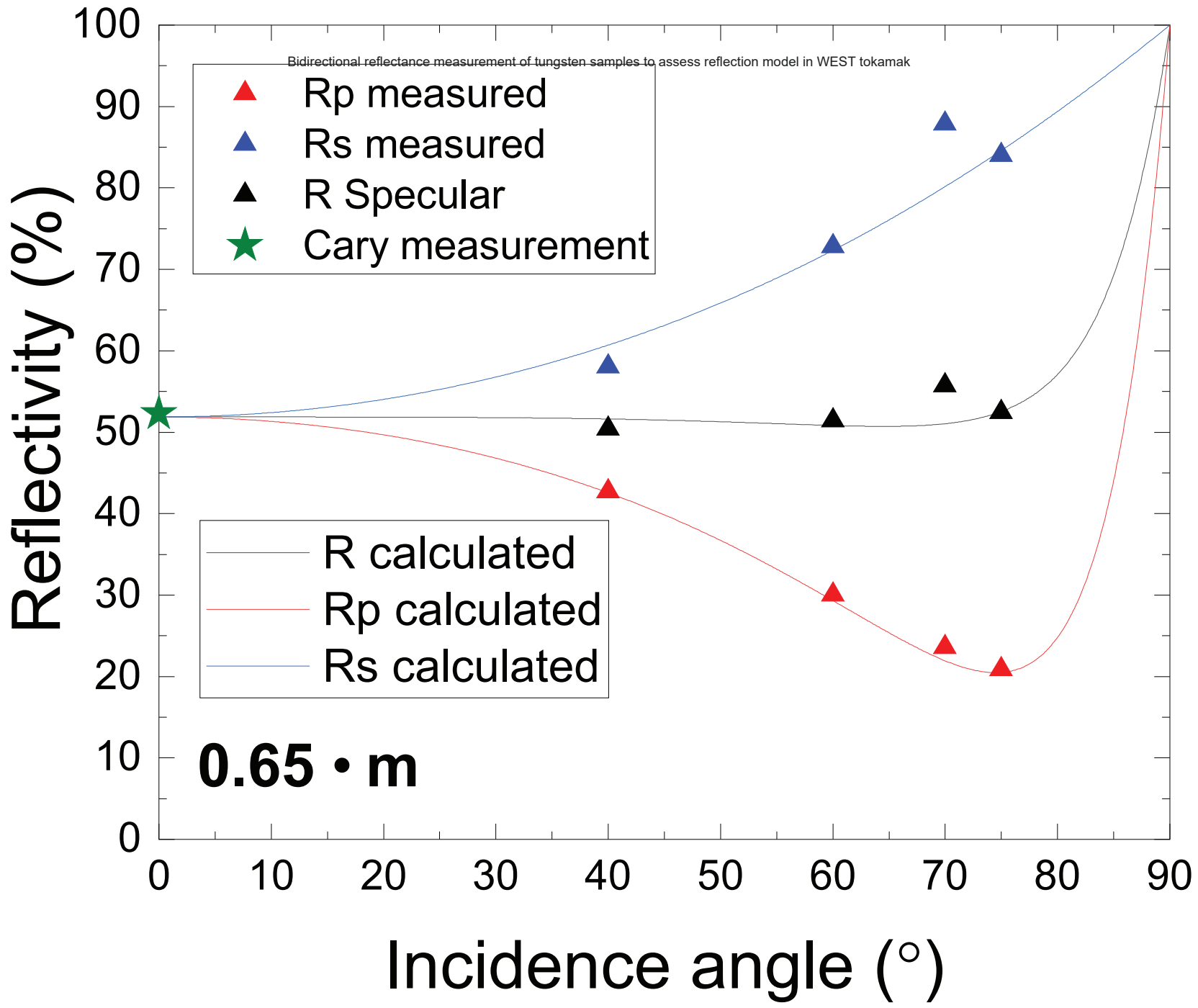
Bidirectional reflectance measurement of tungsten samples to assess reflection model in WEST tokamak
Rp measured
Rs measured
R Specular
Cary measurement
R calculated
Rp calculated
Rs calculated
0.65 • m
Reflectivity (%)
Incidence angle (°)
0
10
20
30
40
50
60
70
80
90
100

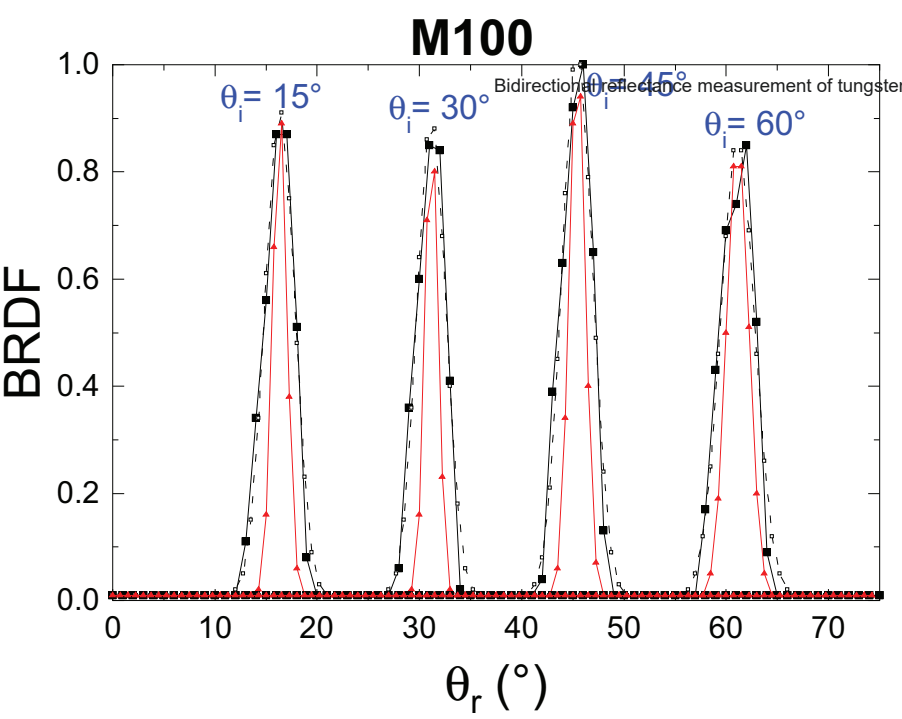
M100
BRDF
θr (°)
θi= 15°
θi= 30°
θi= 45°
θi= 60°

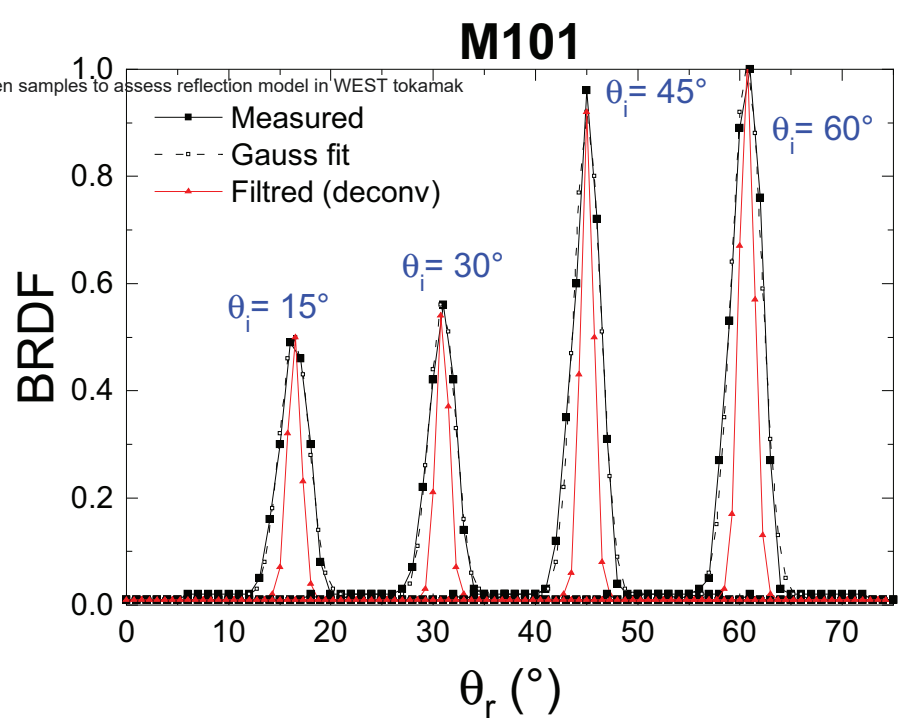
M101
BRDF
θr (°)
Measured
Gauss fit
Filtred (deconv)
θi= 15°
θi= 30°
θi= 45°
θi= 60°

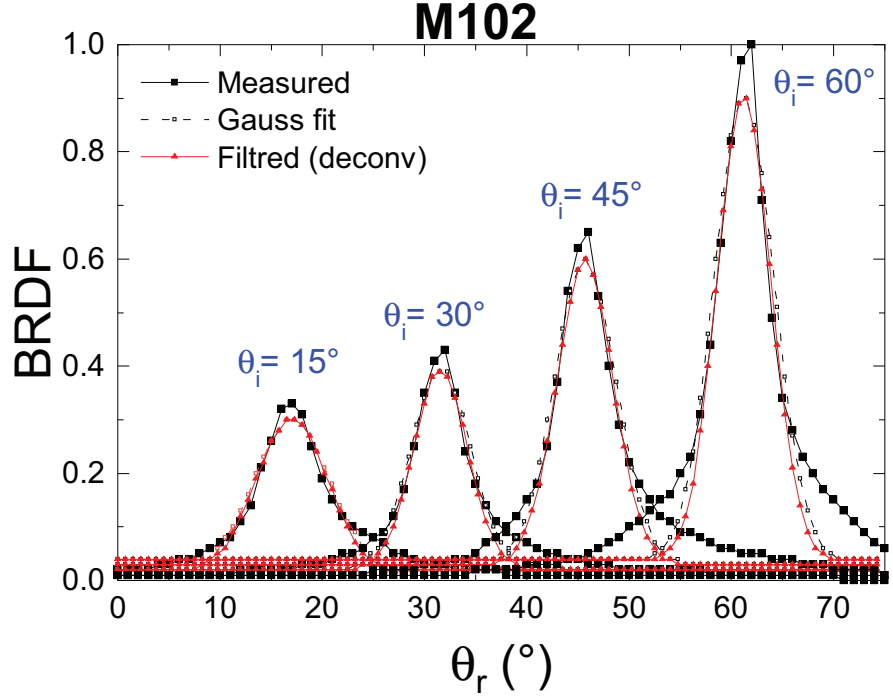
M102
BRDF
θr (°)
Measured
Gauss fit
Filtred (deconv)
θi= 15°
θi= 30°
θi= 45°
θi= 60°

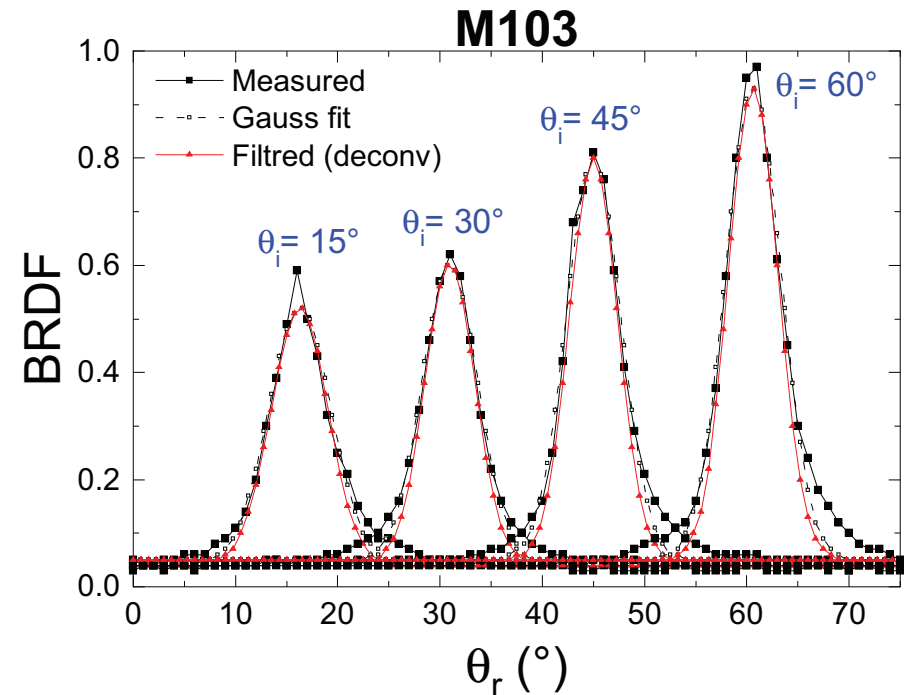
M103
BRDF
θr (°)
Measured
Gauss fit
Filtred (deconv)
θi= 15°
θi= 30°
θi= 45°
θi= 60°

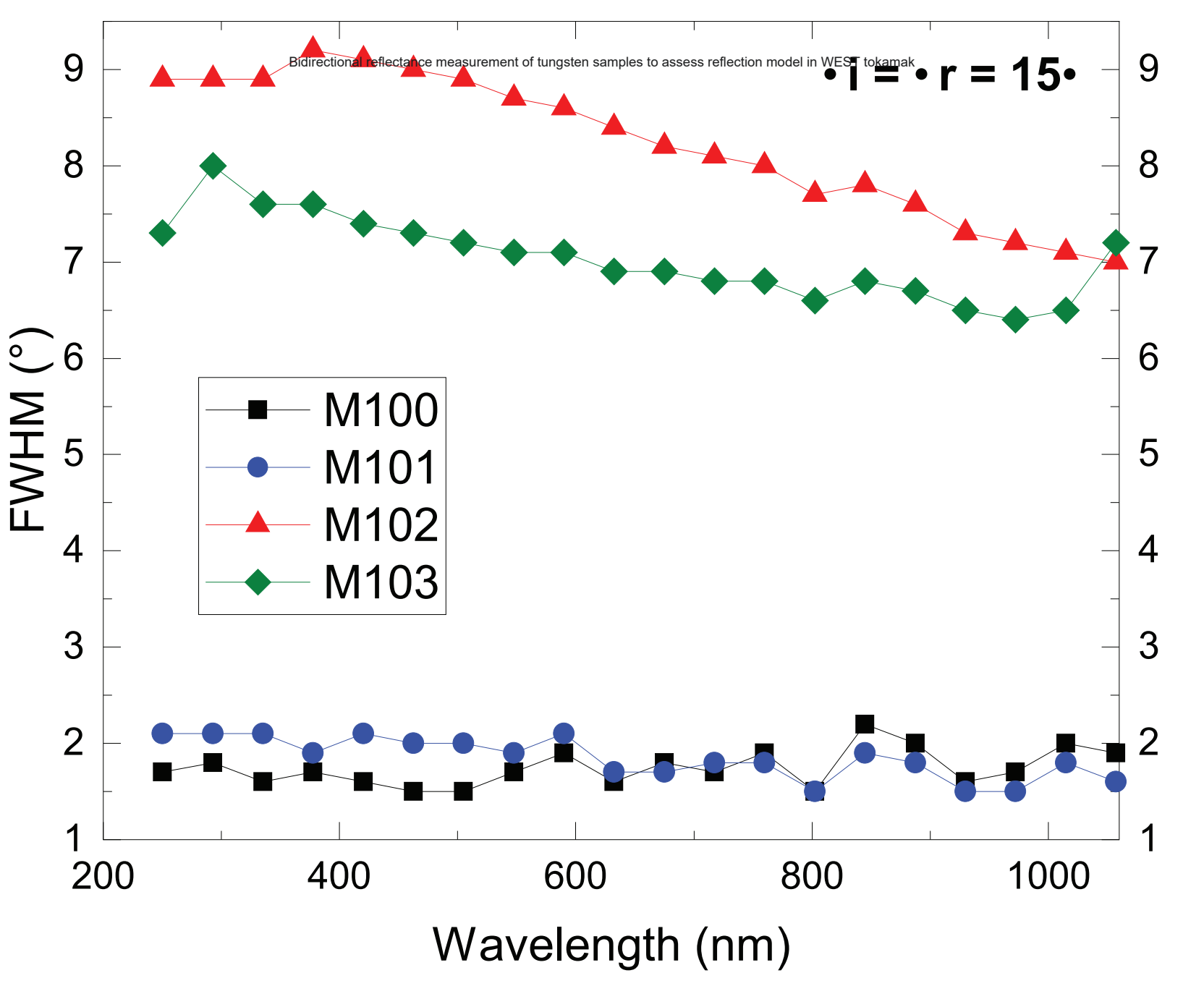
Bidirectional reflectance measurement of tungsten samples to assess reflection model in WEST tokamak
•i = • r = 15•
M100
M101
M102
M103
FWHM (°)
Wavelength (nm)
1
2
3
4
5
6
7
8
9
200
400
600
800
1000

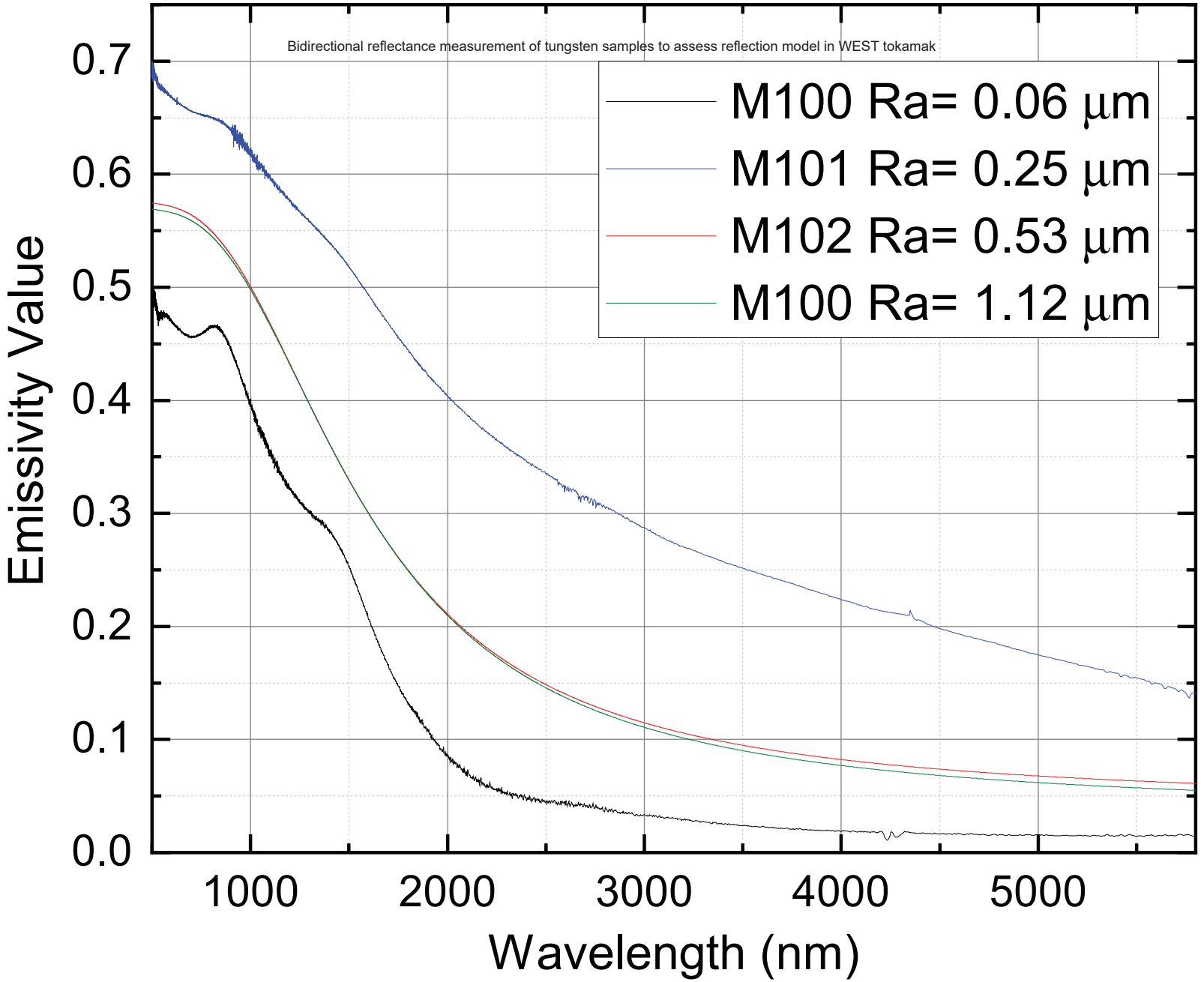
Bidirectional reflectance measurement of tungsten samples to assess reflection model in WEST tokamak
M100 Ra= 0.06 µm
M101 Ra= 0.25 µm
M102 Ra= 0.53 µm
M100 Ra= 1.12 µm
Emissivity Value
0.0
0.1
0.2
0.3
0.4
0.5
0.6
0.7
1000
2000
3000
4000
5000
Wavelength (nm)

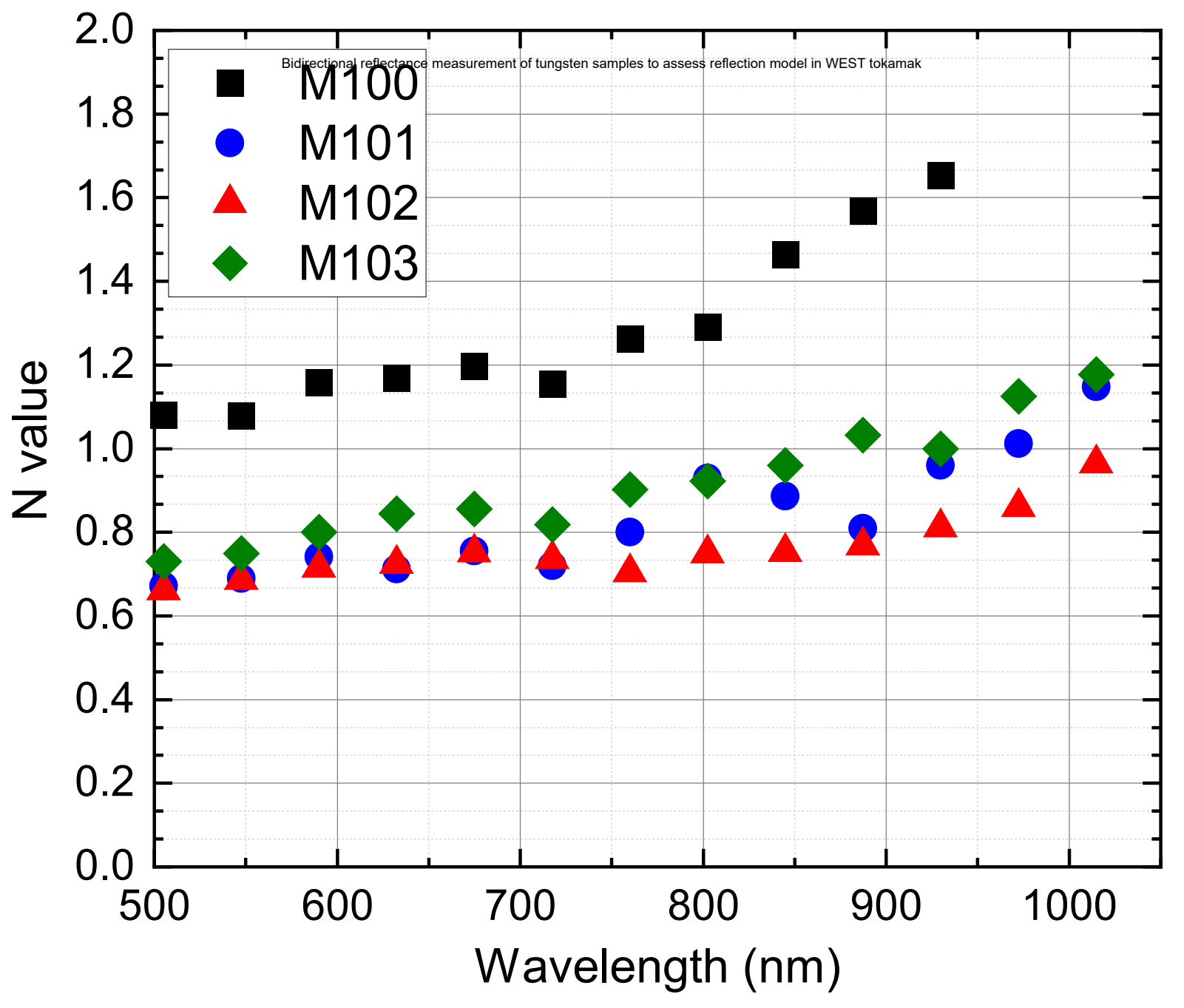
Bidirectional reflectance measurement of tungsten samples to assess reflection model in WEST tokamak
M100
M101
M102
M103
N value
Wavelength (nm)
2.0
1.8
1.6
1.4
1.2
1.0
0.8
0.6
0.4
0.2
0.0
500
600
700
800
900
1000

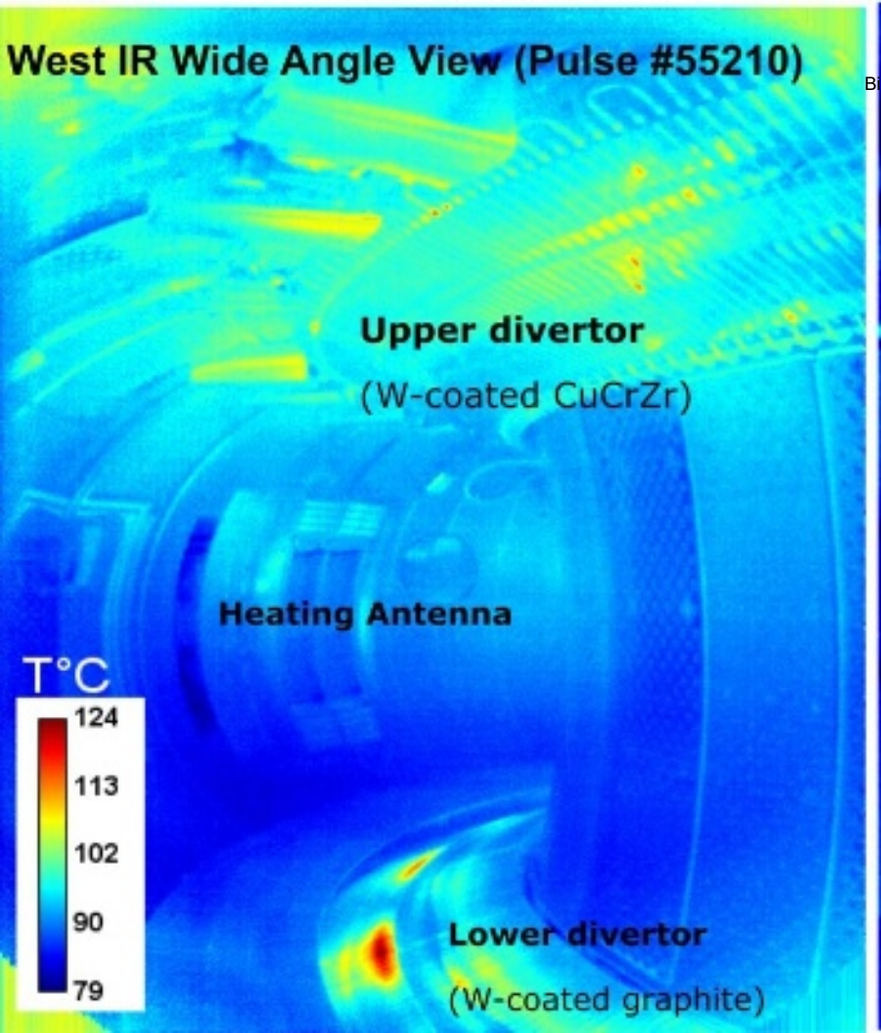

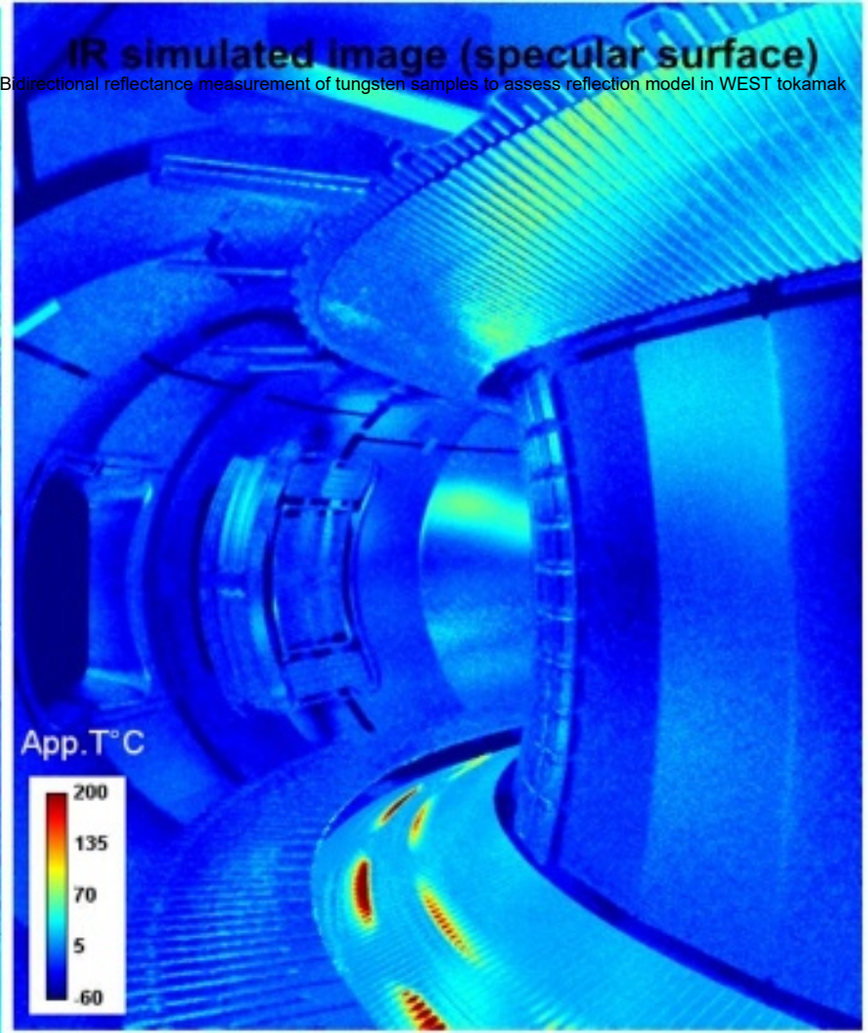

Bidirectional reflectance measurement of tungsten samples to assess reflection model in WEST tokamak